Supporting Information

Characterization of a new bio-based and biodegradable blends of poly(3-hydroxybutyrate-co-3-hydroxyvalerate) and poly(butylene-co-succinate-co-adipate)

Benjamin Le Delliou[1], Olivier Vitrac[1], Mickael Castro[2], Stephane Bruzaud[2], Sandra Domenek[1,a]

[1]UMR 0782 SayFood Paris-Saclay Food and Bioproduct Engineering Research Unit, INRAE, AgroParisTech, Université Paris-Saclay, 91300, Massy France

[2]University Bretagne Sud, UMR CNRS 6027, IRDL, F- 56100 Lorient, France

[a]Corresponding author: Sandra Domenek, 1 rue des Olympiades, 91300 Massy, France
sandra.domenek@agroparistech.fr

S.1: Internal mixing of PHBV/PBSA blends

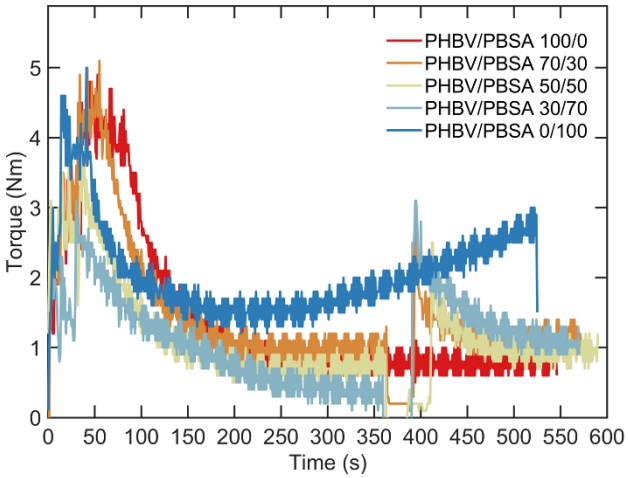

Figure S1.1. Evolution of torque during melt mixing of PHBV/PBSA blends

PHBV/PBSA blend behavior during mixing was assessed by monitoring the torque evolution over time for five PBSA ratios as shown in Figure S1.1. During the first 300 s, pure PHBV exhibited an exponential torque decay down to a plateau below 1 N·m controlled by its viscosity at molten state. After melting, PHBV/PBSA blend showed stable torque at ca. 1 N·m independent of PBSA content. Comparatively, the torque of pure PHBV was twice higher due to its higher melt viscosity.

S.2: Thermo-gravimetric analysis of PHBV/PBSA blends

The thermal stability of the blends was assessed by Thermo-Gravimetric Analysis (TGA, Q500, TA Instruments). The experiment was performed from +25 °C to +450 °C in high resolution mode where the heating rate is controlled by the decomposition rate of the sample. An average weight of 10 mg was used each time.

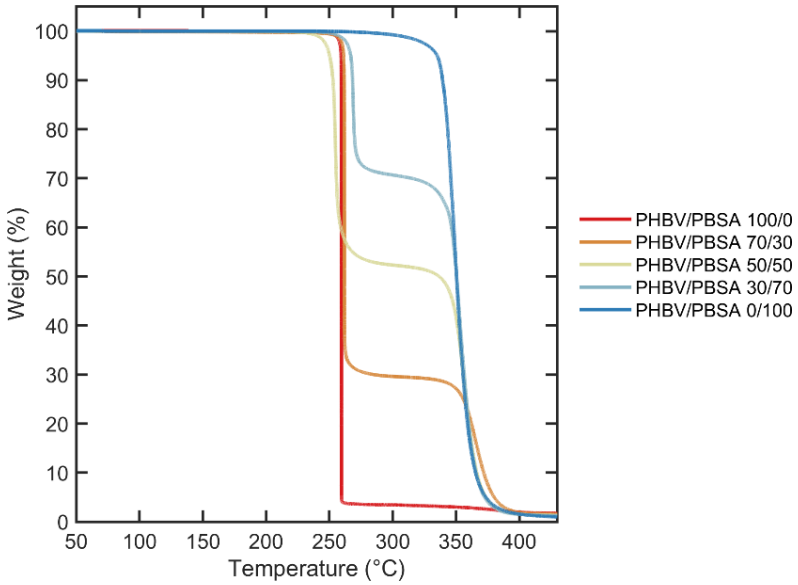

Figure S2.1. Thermogravimetric analysis of neat PHBV, neat PBSA and PHBV/PBSA blends

The thermo-gravimetric analysis was used to confirm the weight ratio of PBSA in the PHBV/PBSA blends. In fact, PHBV and PBSA have two distinct degradation temperatures which was used to confirm the initial ratio of PBSA phase in the blend as shown in Figure S2.1. Secondly, thermo-gravimetric analysis was used to study the thermal stability of the blends depending on the PBSA content added. Both PHBV and PBSA show a single step decomposition. PHBV degrades at about 250 °C and presents a high degradation rate while PBSA degrades at a temperature of about 350 °C with slower kinetics. PHBV/PBSA blend curves present two degradation steps where the first step is correlated to the degradation of the PHBV phase and the second one at higher temperature to the PBSA phase.

S.3: Thermal stability of PHBV

The thermal stability of PHBV was assessed following a dynamic time sweep test during 1 h at 0.1 % and 1 Hz. As shown in Figure S3.1 after 20 min, the complex viscosity dropped by decade from 1238 Pa.s to 92 Pa.s. PHBV undergoes rapid thermal degradation showing poor thermal stability. This behavior was expected given the very narrow processing window of PHBV and was already observed by Gerard. [1]

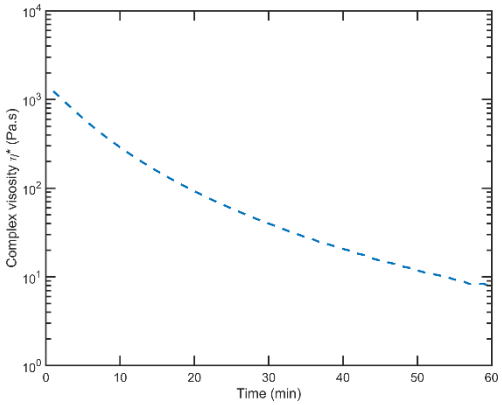

Figure S3.1. Study of the thermal stability of PHBV with evolution the complex viscosity in time at strain 0.1 %, frequency 1 Hz and T= 185 °C

S.4: Determination of the equilibrium melting temperature T_m^0

Program III, Figure S4.1, monitored crystallization kinetics at different temperatures. Samples were quenched down to the desired crystallization temperature from the melt: 120 °C, 110 °C, 100 °C and 90 °C. Crystallization kinetics were recorded isothermally until equilibrium. Corresponding melting temperatures were analyzed during heating to 190 °C at 10 °C/min.

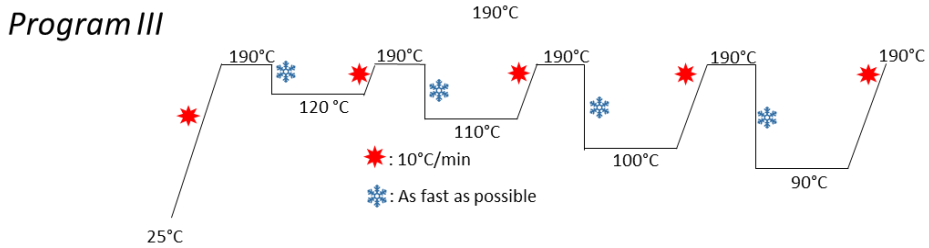

Figure S4.1. Schematic representation of DSC protocol of Program III

The equilibrium melting temperature T_m^0 of PHBV in blends was determined by following the Hoffman-Weeks (H-W) method [2] after heating the crystallized samples at 10 °C/min. Collected melting temperatures T_m were plotted against crystallization temperatures, as shown in Figure S4.2. The evolution is extrapolated linearly until intercepting the line $T_m = T_C$

which identifies the condition $T_m = T_m^0$. The obtained values with H-W method are gathered in Table S4.1. For neat PHBV, T_m^0 was found equal to 175 °C in agreement with the previous determination of 178 °C ± 5 °C reported with PHBV-3HV% (ENMAT Y1000, Tianan Biopolymer, China).[3] T_m^0 values in PHBV/PBSA blends were similar, except for PHBV/PBSA 30/70, whose value shifted to 182 °C.

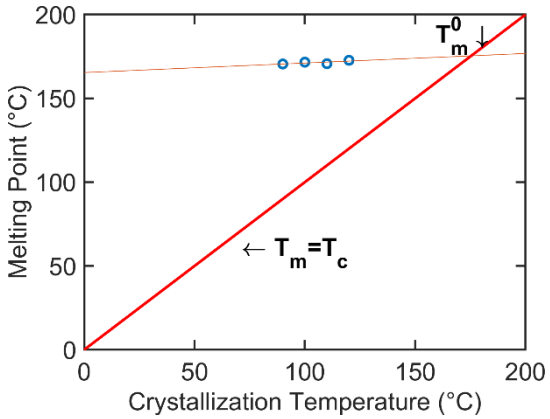

Figure S4.2. Determination of equilibrium melting temperature from isothermal crystallization kinetics, example shown for neat PHBV sample

Table S4.1. Equilibrium melting temperature from isothermal crystallization kinetics

Samples		T_m^0 (°C)
PHBV/PBSA	100/0	175
	70/30	175
	50/50	174
	30/70	182
	0/100	n.d

S.5: Non-isothermal crystallization of PHBV/PBSA blends

The non-isothermal crystallization kinetics were analyzed by DSC. The raw data are shown in the Figure S5.1.

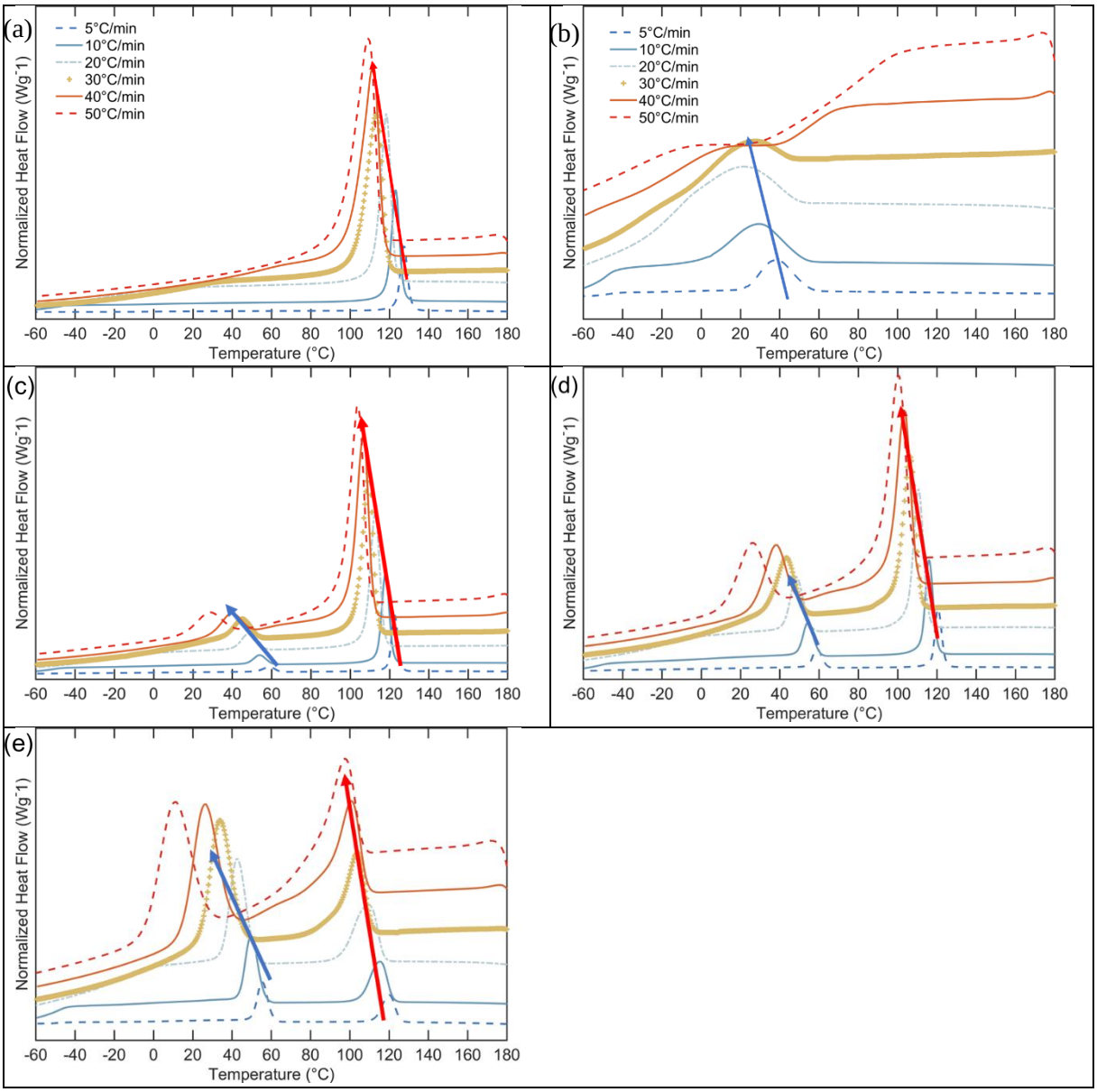

Figure S5.1. DSC curves for non-isothermal crystallization at various cooling rate of (a) neat PHBV, (b) neat PBSA and PHBV/PBSA blends, i.e. (c) 70/30, (d 50/50), (e) 30/70

Table S5.1. Raw data of the crystallization enthalpy measured by DSC and displayed in Figure S5.1.

Raw data

	H_c of PHBV phase (J/g)						H_c of PBSA phase (J/g)					
	5 °C/min	10 °C/min	20 °C/min	30 °C/min	40 °C/min	50 °C/min	5 °C/min	10 °C/min	20 °C/min	30 °C/min	40 °C/min	50 °C/min
PHBV	95	91	86	82	91	86						
PBSA							52	49	22	4	*0*	*0*
PHBV/PBSA 70/30	68	65	62	56	55	57	13	13	13	16	9	7
PHBV/PBSA 50/50	36	46	40	44	40	44	24	24	26	23	18	14
PHBV/PBSA 30/70	25	26	24	22	23	26	39	39	47	41	27	24

Values corrected by the weight percentage of each polymer

	$H_{c,corr}$ of PHBV phase (J/g)						$H_{c,corr}$ of PBSA phase (J/g)					
	5 °C/min	10 °C/min	20 °C/min	30 °C/min	40 °C/min	50 °C/min	5 °C/min	10 °C/min	20 °C/min	30 °C/min	40 °C/min	50 °C/min
PHBV	95	91	86	82	91	86						
PBSA							52	49	22	4	0	0
PHBV/PBSA 70/30	97	93	88	80	79	82	42	42	42	55	28	22
PHBV/PBSA 50/50	72	93	80	89	81	87	48	48	53	46	35	28
PHBV/PBSA 30/70	82	86	82	72	77	87	56	56	67	59	38	35

S.6: Avrami-Jeziorny analysis of non-isothermal crystallization kinetics

The relative crystallinity degree (χ), as a function of temperature (T), is calculated from the energy released over the nonisothermal crystallization process using the running integral of the crystallization enthalpy recorded by DSC. It can be defined by Equation S1 :

$$\frac{\int_{T_0}^{T}\left(\frac{dH_c}{dT}\right)dT}{\int_{T_0}^{T\infty}(dH_c/dT)dT}, \quad (1)$$

where T_0 and T represent the onset and end of crystallization temperature, respectively and dH_c is the measured enthalpy of crystallization for an infinitesimal temperature range dT.

Since it can be considered that the difference between the sample temperature and DSC furnace is negligible, then the relative crystallinity versus time can be obtained from Equation S2 , where α is the cooling rate (°C/min) and t represents time (min):

$$t = \frac{T_0 - T}{\alpha}, \quad (2)$$

The relative degree of crystallinity versus time for PHBV/PBSA blends is represented in **Figure S**.1(a) and **Figure S**.1(b) for PHBV and PBSA phase, respectively. All curves showed a sigmoidal profile with a linear part between 0.2 and 0.6 % relative crystallinity. The Avrami-Jeziorny analysis of non-isothermal crystallization kinetics was carried out within this range. All obtained values for Avrami constants n_a, k_a and k_c are gathered in Table S6.1.

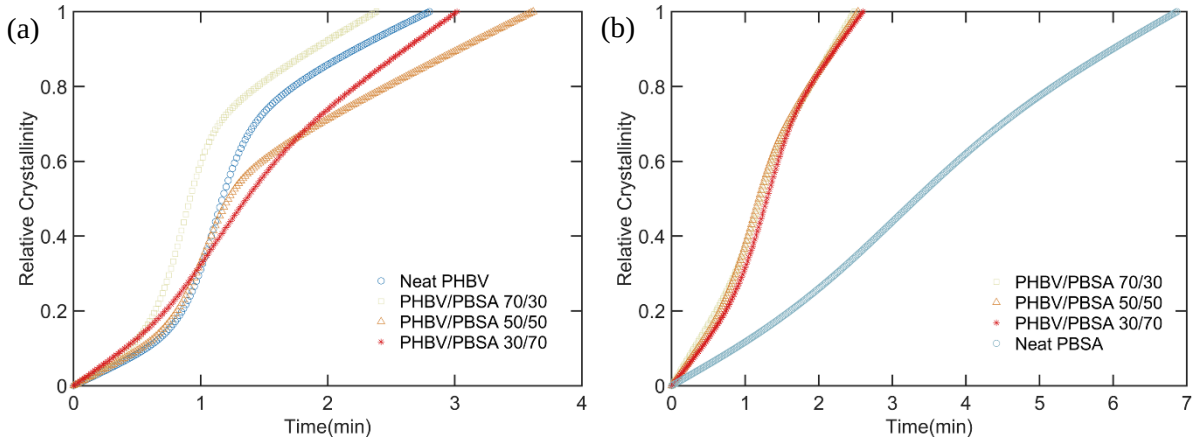

Figure S6.1. Variation of relative crystallinity versus crystallization time for PHBV/PBSA blend ratios related to a) PHBV phase and b) PBSA phase for non-isothermal crystallization at 10°C/min

The study of the crystallization kinetics was conducted using the most common model to describe the overall isothermal crystallization that is the Avrami model.[4-6] It relates on the relative crystallinity as a function of time following Equation S3 :

$$\chi(t) = 1 - \exp(-k_a t^{n_a}) \in [0,1] \quad (3)$$

By taking the double logarithmic form of Equation S3 , then it can be transformed into Equation S4 :

$$\log\big(-\ln\big(1-\chi(t)\big)\big) = \log k_a + n_a \log t\,, \quad (4)$$

where k_a is the Avrami crystallization rate constant and n_a the Avrami exponent which gives information about nucleating and growth geometry.

Both Avrami parameters, n_a and k_a, can be obtained from the slope and interecept of the as-defined linear portion of l*og(-ln(1-X(T))* versus *log t*, respectively (Figure S6.2a,b).

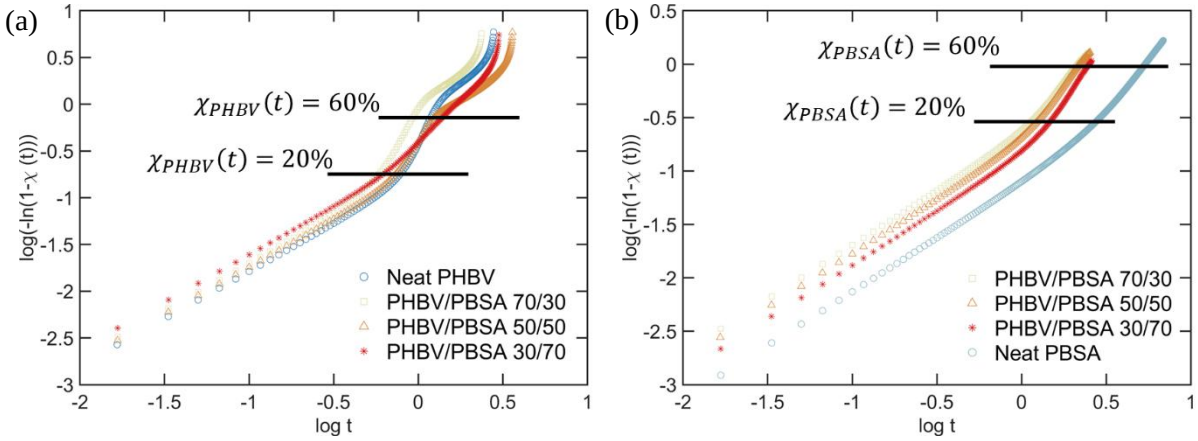

Figure S6.2. Plots of log(-ln(1-X(T)) versus log t for non isothermal crystallization at 10°C/min for PHBV/PBSA blend with a) PHBV phase and b) PBSA phase

Given the non-isothermal conditions and based on Jeziorny recommendations the value k_a should be corrected by taking into account the cooling rate as introduced in Equation S5 : [7]

$$\log k_c = \frac{\log k_a}{\alpha} \quad (5)$$

From the fitted Avrami-Jeziorny parameters the half time of crystallization $t_{1/2,c}$ can be estimated according to Equation S6 :

$$\mathrm{t}_{1/2,\mathrm{c}} = \left(\frac{\ln 2}{k_c}\right)^{1/n_a} \quad (6)$$

For both phases, the rate constant k_c increased from 5 °C/min to 20 °C/min while no change was observed for higher cooling rate with value close to 1. Evaluation of n_a brings an information on the type of homogeneous or heterogeneous nucleation. In non-isothermal crystallization kinetic studies, n_a values can be used to compare systems. A decrease in n_a of PHBV was observed with incorporation of PBSA, indicating a diminishing of the dimension of crystallization. The $F(T)$ values of PBSA phase remained stable.

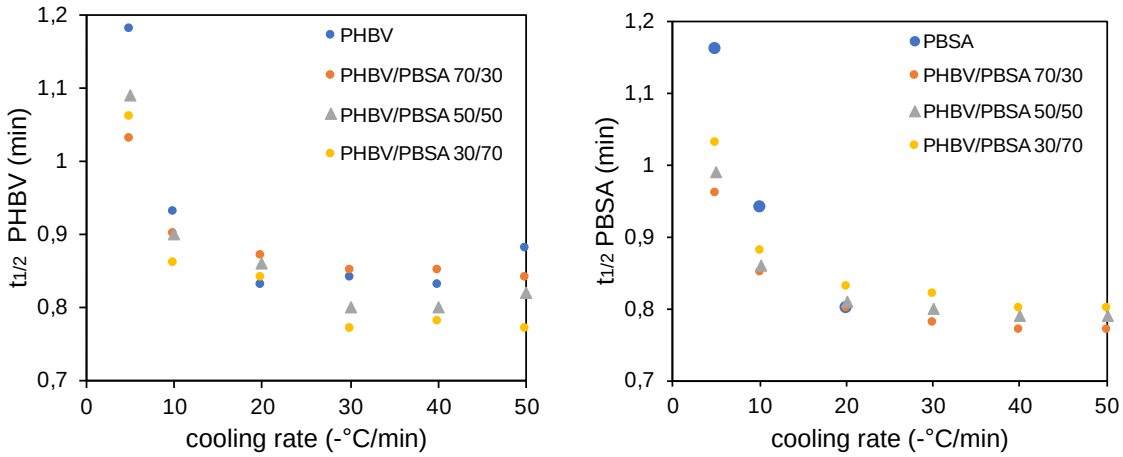

Figure S6.3. Graphical representation of the non-isothermal crystallization half-times of PHBV (left) and PBSA (right) in PHBV/PBSA blends calculated with the help of the Avrami-Jeziorny analysis.

Table S6.1. Avrami–Jeziony parameters during nonisothermal crystallization of neat PHV, neat PBSA and PHBV/PBSA blends

Materials	Cooling	n	Ka	Kc	n	Ka	Kc
PHBV	5	4.6	0	0.3	n.d	n.d	n.d
	10	3.7	0.38	0.9	n.d	n.d	n.d
	20	2.1	1.14	1	n.d	n.d	n.d
	30	2.4	4.91	1.1	n.d	n.d	n.d
	40	2.2	7.63	1.1	n.d	n.d	n.d
	50	3.6	33.2	1.1	n.d	n.d	n.d
PBSA	5	n.d	n.d	n.d	1.8	0.04	0.5
	10	n.d	n.d	n.d	1.5	0.06	0.8
	20	n.d	n.d	n.d	1.5	0.2	0.9
	30	n.d	n.d	n.d	1.3	0.7	1
	40	n.d	n.d	n.d	-	-	-
	50	n.d	n.d	n.d	-	-	-
PHBV:	5	3.7	0.1	0.6	1.9	0.2	0.7
PBSA	10	3.2	0.91	1	1.4	0.3	0.9
70/30	20	3	3.25	1.1	1.7	1.5	1
	30	2.6	6.41	1.1	1.6	2.1	1
	40	2.5	9.18	1.1	1.5	2.3	1
	50	2.3	10.3	1.1	1.5	2.6	1
PHBV:	5	3.5	0.03	0.5	2.1	0.2	0.7
PBSA	10	2.5	0.4	0.9	1.5	0.2	0.9
50/50	20	2.6	1.29	1	1.9	1.4	1
	30	1.7	1.78	1	1.8	1.9	1
	40	1.8	2.33	1	1.7	2.2	1
	50	2	3.77	1	1.6	2.5	1
PHBV:	5	1.6	0.1	0.6	2.3	0.1	0.7
PBSA	10	1.8	0.4	0.9	1.4	0.2	0.8
30/70	20	2	2.5	1	2	0.9	1
	30	1.5	1.3	1	1.9	1.3	1
	40	1.5	1.7	1	1.8	1.8	1
	50	1.4	1.9	1	1.7	2	1

To go further in the kinetic analysis of the present study, the model developed by Liu et al.,[8] was investigated. Liu's model combines the Avrami and Ozawa model[9] which was developed by Ozawa et al.,[9] from the Avrami equation. The degree of conversion at temperature T amounts to Equation S7:

$$\chi(\mathrm{T}) = 1 - \exp\left(-\frac{k_0}{\alpha^{n_0}}\right), \quad (7)$$

where k_0 and n_0 are the Ozawa rate constant and exponent, respectively and α the constant cooling rate. Then by taking the double logarithmic form of Equation S7, then it can be transformed into Equation S8 :

$$\log\left(-\ln\left(1-\chi(\mathrm{T})\right)\right) = \log k_0 - m_0 \log \alpha, \quad (8)$$

where m is the ratio of the Ozawa and the Avrami exponent ($m = n_a/m_o$).

The Liu and Mo model is defined as the combination of the double logarithmic form of the Avrami and Ozawa,[8] which gives Equation S9 :

$$log k_a - \mathrm{n_a} \log \mathrm{t} = \log k_0 - m_0 \log \alpha, \quad (9)$$

and rewritten as Equation S10 :

$$\log \alpha = \log F(T) - m \log t \ , \quad (10)$$

where $F(T)$= $[(k_0/k_c)^{\frac{1}{n_0}}$ and as previously said m is the ratio of the Ozawa and the Avrami exponent ($m = n_a/m_o$).

The $\log \alpha$ vs $\log t$ was plotted and obtained results are available in Figure S6.3(a-d) and Figure S6.4(a-d) for PHBV and PBSA phases, respectively.

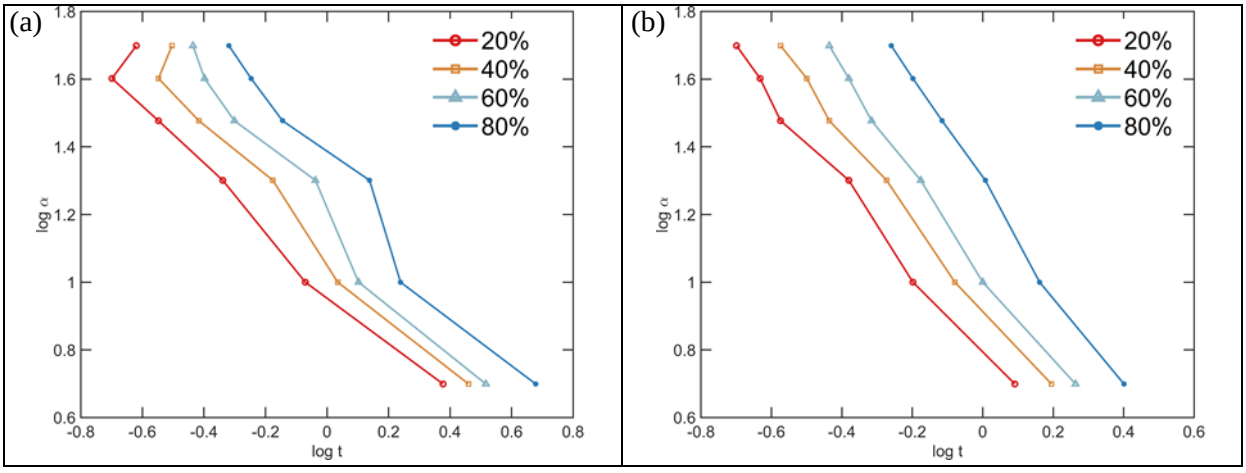

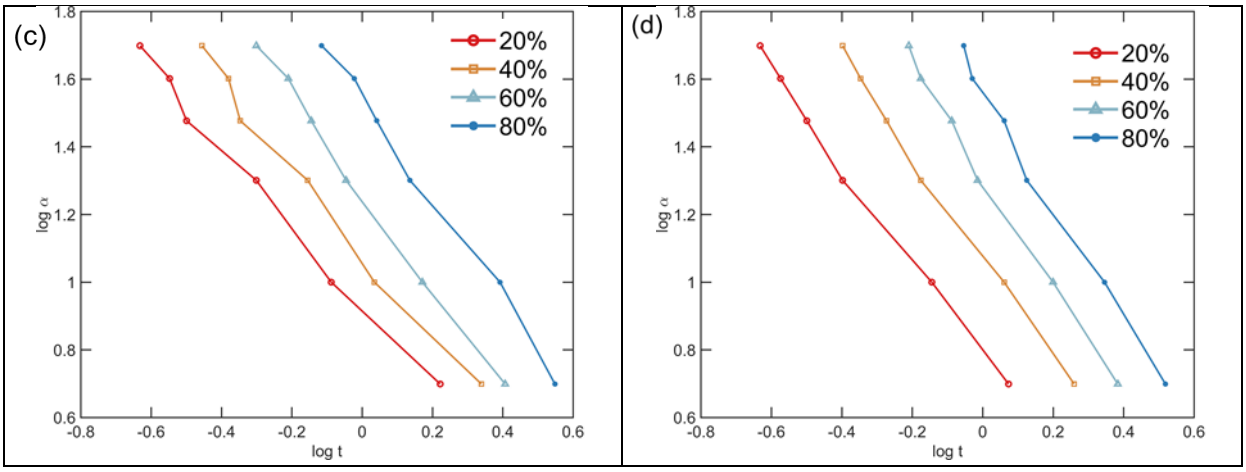

Figure S6.3. Plots of *log α* versus *log t* for non-isothermal crystallization for PHBV-phase of (a) Neat PHBV, (b) PHBV/PBSA 70/30, (c) PHBV/PBSA 50/50 , (d) PHBV/PBSA 30/70

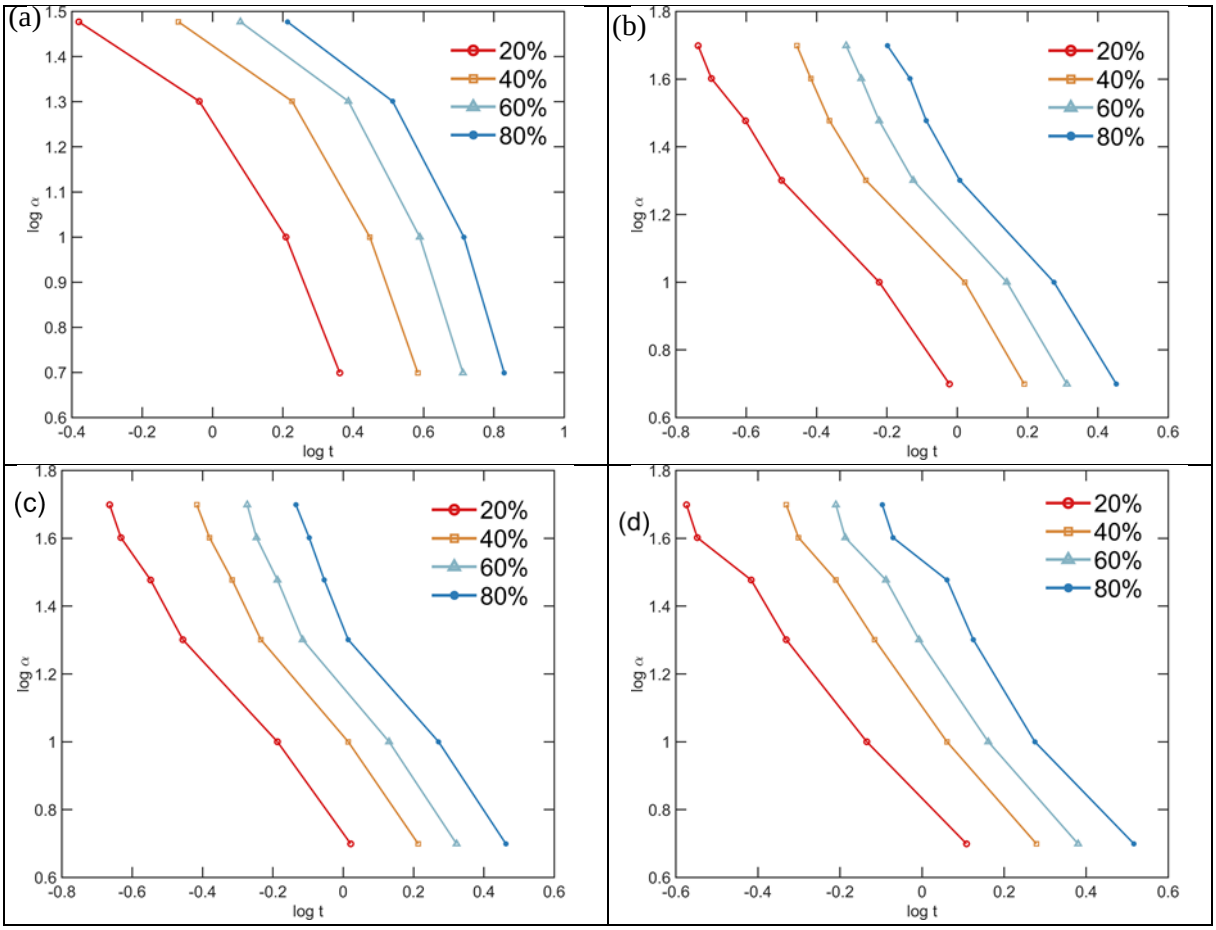

Figure S6.4. Plots of *log α* versus *log t* for non-isothermal crystallization for PBSA-phase of (a) Neat PBSA, (b) PHBV/PBSA 70/30, (c) PHBV/PBSA 50/50 , (d) PHBV/PBSA 30/70

S.7: Dynamic mechanical analysis

Table S7.1. Determination of Storage Modulus *E'* and T_α values of PHBV/PBSA blends obtained from DMA

Samples		Tα[(1)]	
		PHBV	PBSA
PHBV/PBSA	100/0	19.6	n.d
	70/30	19.5	-35
	50/50	21.7	-33
	30/70	23.8	-33
	0/100	n.d	-35

(1) Determined as the maximum value of the tan δ peaks

The dynamic glass transition temperature determined as the maximum value of the *tan* δ peaks is reported in Table S7.1. As expected, two distinct relaxation temperatures were observed because of immiscibility of PHBV and PBSA, which is coherent with previous observations from DSC. The T_a attributed to PHBV and PBSA could reasonably described as stable since no significant shift towards lower and higher temperatures was observed for PHBV and PBSA phase, respectively. Hence, this result brings further confirmation that PHBV and PBSA components are both immiscible.

S.8: Stress-oscillation behavior of PBSA from tensile test

File with video

S.9: Equivalent box model

In the present study, prediction of the elastic modulus was monitored using the Equivalent Box Model (EBM). Simple prediction of the physical properties can be modelled with the Reuss (parallel resistances), Voigt (serial resistances):

$$E^n = \phi_1 E_1^n + \phi_2 E_2^n \quad (11)$$

where $E_1$and E_2 are the elastic modulus of phase 1 and 2, ϕ_1 and ϕ_2 the volume fraction of phase 1 and phase 2, and exponent *n* characterizes the type of model with *n=1* (Parallel or Reuss model), *n=-1* (Series or Voigt model)

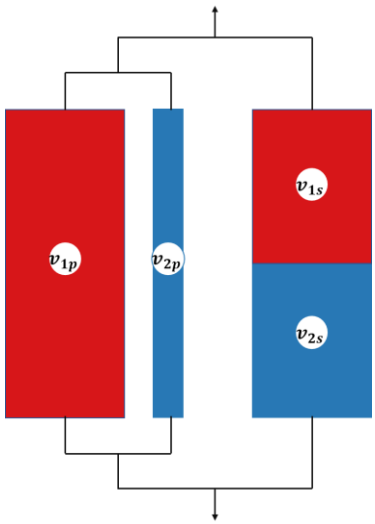

Figure S9.1. Schematic representation of an equivalent box model (EBM) for a binary blend

More complex models can be required since representation of the mechanical properties with simple parallel or series model cannot be accurately used. Equivalent box model (EBM) relates on the existence of two volume fractions where a volume fraction that acts in parallel and a volume fraction that acts in series (Figure S9.1).[10] The EBM model is a two-parameter model, as of four volume fraction v_{ij}, only two are independent [11]. The fractions are linked as follows:

$$v_p = v_{1p} + v_{2p} \qquad v_s = v_{1s} + v_{2s}$$
$$v_1 = v_{1p} + v_{1s} \qquad v_2 = v_{2p} + v_{2s} \qquad (12)$$
$$v_1 + v_2 = v_p + v_s = 1$$

where v_p and v_s are the total volume fractions of the parallel branch and series branch, respectively.

The tensile moduli of the parallel (E_p) and series (E_s) branches of the EBM can be expressed by following equations:

$$E_p = \frac{E_1 v_{1p} + E_2 v_{2p}}{v_p} \qquad E_s = \frac{v_s}{\frac{v_{1s}}{E_1} + \frac{v_{2s}}{E_2}} \qquad (13)$$

where E_1 and E_2 are the Young's moduli of phases 1 and 2, respectively.

The resulting tensile modulus of two components blend (E_b) is then given as the sum $E_p v_p + E_s v_s$ [10]:

$$\mathrm{E_b} = \mathrm{E_1 v_{1p}} + \mathrm{E_2 v_{2p}} + \mathrm{v_s^2}/(\frac{\mathrm{v_{1s}}}{\mathrm{E_1}} + \frac{\mathrm{v_{2s}}}{\mathrm{E_2}}) \qquad (14)$$

The main issue comes from the evaluation of v_{ij}. From percolation theory,[12] the contribution of one component is negligible and gives:

$$E_{1b} = E_0(v_1 - v_{1cr})^q \quad (15)$$

where E_0 is a constant, q is the critical exponent, which assumes a value of 11/6 for a three-dimensional lattice[12].

From experimental results,[12,13] it has been shown that Equation S15 can plausibly fit the experiment data for blends in the range $v_{1cr} < v_1 < 1$ (where $E_1 >> E_2$) so that the modulus of the neat component 1 can be expressed as follows:

$$E_1 = E_0(v_1 - v_{1cr})^{q1}, \quad (16)$$

which gives:

$$E_{1b} = E_1[v_1 - v_{1cr})/(1 - v_{1cr})]^{q1}. \quad (17)$$

Based on the percolation theory, where the assumption that the contribution of the second component can be negligible then if $E_1 > > E_2$, the contribution $E_2 v_{2p}$ of component 2, which is coupled in parallel, and the contribution of the whole series branch to the modulus of the EBM are negligible in comparison with the contribution the $E_1\ v_{1p}$ of component 1. Consequently, $E_1\ v_{1p}$ (or $E_2\ v_{2p}$ for $E_2 > > E_1$) can be set equal to the apparent modulus E_{1b} (or E_{2b} for $E_2 > > E_1$) where:

$$E_{1b} = E_1 v_{1p} \qquad E_{2b} = E_2 v_{2p}. \quad (18)$$

Hence, combination of Equation S16 and Equation S17 gives:

$$v_{1p} = [\frac{v_1 - v_{1cr}}{(1 - v_{1cr})}]^{q1} \qquad v_{2p} = [\frac{v_2 - v_{2cr}}{(1 - v_{2cr})}]^{q2}. \quad (19)$$

In the marginal zone, *i.e.* $0<v_1<v_{1cr}$ (or $0<v_2<v_{2cr}$), it can be set for the minority component that v_{1p}=0 and v_{1s}=v_1 (or v_{2p}=0 and v_{2s}=v_2).

For discrete domain of spherical form, the percolation threshold can be set to $v_{1cr} = v_{2cr} = 0.156$.[10,14] Most experimental values of q are located in the interval 1.6-2 so that $q = 1.8$ can be used as an average value.[11]

Moreover, prediction of strength can be modeled from Equation S20:[15]

$$S_b = S_1 v_{1p} + S_2 v_{2p} + A S_2 v_s, \quad (20)$$

where S_1>S_2, S_1 and S_2 are the strength of phase 1 and 2, respectively. While A can be identified as level of interfacial bonding.

Two limiting values of S_b can be identified with lower and upper bound where A= 0 or 1 depending on level of interfacial adhesion either very weak or strong enough to transmit the acting stress between constituents. Consequently, for A=0, series branch does not contribute and resulting S_b is equal to the sum of contributions of parallel element. While for A=1, contribution of series branch is added to that of the parallel branch. [10,11]

References

1. T. Gerard, T. Budtova, *European Polymer Journal* **2012**, *48*, 1110, https://doi.org/10.1016/j.eurpolymj.2012.03.015.
2. J. D. Hoffman, J. J. Weeks, *Journal of Research of the National Bureau of Standards Section a-Physics and Chemistry* **1962**, *66*, 13, 10.6028/jres.066A.003.
3. J. A. S. Puente, A. Esposito, F. Chivrac, E. Dargent, *Macromolecular Symposia* **2013**, *328*, 8, 10.1002/masy.201350601.
4. M. Avrami, *The Journal of Chemical Physics* **1941**, *9*, 177, 10.1063/1.1750872.
5. M. Avrami, *The Journal of Chemical Physics* **1940**, *8*, 212, 10.1063/1.1750631.
6. M. Avrami, *The Journal of Chemical Physics* **1939**, *7*, 1103, 10.1063/1.1750380.
7. A. Jeziorny, *Polymer* **1978**, *19*, 1142, https://doi.org/10.1016/0032-3861(78)90060-5.
8. T. Liu, Z. Mo, S. Wang, H. Zhang, *Polymer Engineering & Science* **1997**, *37*, 568, https://doi.org/10.1002/pen.11700.
9. T. Ozawa, *Polymer* **1971**, *12*, 150, https://doi.org/10.1016/0032-3861(71)90041-3.
10. J. Kolarik, *Polym. Eng. Sci.* **1996**, *36*, 2518, 10.1002/pen.10650.
11. Y. J. Phua, A. Pegoretti, T. M. Araujo, Z. A. M. Ishak, *Journal of Applied Polymer Science* **2015**, *132*, 10.1002/app.42815.
12. P.-G. De Gennes, *Journal de Physique Lettres* **1976**, *37*, 1, 10.1051/jphyslet:019760037010100.
13. J. Lyngaae-Jorgensen, A. Kuta, K. Sondergaard, K. V. Poulsen, *Polym. Networks Blends* **1993**, *3*, 1.
14. L. A. Utracki, *J. Rheol.* **1991**, *35*, 1615, 10.1122/1.550248.
15. J. Kolařík, *Polymer* **1996**, *37*, 887, https://doi.org/10.1016/0032-3861(96)87270-3.